

Satellite-based In-situ Monitoring of Space Weather: KSEM Mission and Data Application

Daehyeon Oh, Jiyoung Kim[†], Hyesook Lee, Kun-Il Jang

National Meteorological Satellite Center, Korea Meteorological Administration, Jincheon 27803, Korea

Many recent satellites have mission periods longer than 10 years; thus, satellite-based local space weather monitoring is becoming more important than ever. This article describes the instruments and data applications of the Korea Space wEather Monitor (KSEM), which is a space weather payload of the GeoKompsat-2A (GK-2A) geostationary satellite. The KSEM payload consists of energetic particle detectors, magnetometers, and a satellite charging monitor. KSEM will provide accurate measurements of the energetic particle flux and three-axis magnetic field, which are the most essential elements of space weather events, and use sensors and external data such as GOES and DSCOVR to provide five essential space weather products. The longitude of GK-2A is 128.2° E, while those of the GOES satellite series are 75° W and 135° W. Multi-satellite measurements of a wide distribution of geostationary equatorial orbits by KSEM/GK-2A and other satellites will enable the development, improvement, and verification of new space weather forecasting models. KSEM employs a service-oriented magnetometer designed by ESA to reduce magnetic noise from the satellite in real time with a very short boom (1 m), which demonstrates that a satellite-based magnetometer can be made simpler and more convenient without losing any performance.

Keywords: space weather, geostationary orbit, artificial satellite, payload

1. INTRODUCTION

The lifetimes of artificial satellites have been increasing, and many satellites are now designed to operate in orbit for more than 10 years. Longer operation in space means that satellites will experience more critical space weather events, such as extreme magnetic storms and energetic particle exposure. These events can cause critical satellite anomalies, such as loss of control or data (e.g., Choi et al. 2011; Lohmeyer & Cahoy 2013). Because modern societies are becoming more dependent on satellite-based technologies, satellite anomalies are a critical problem that must be addressed. Ground-based electronic power grids can also be disrupted by space weather. Since the first magnetic storm that affected electronic power and communication systems on March 24, 1940, reported by Davidson (1940) and Nicholson (1940), numerous studies have analyzed the impact of space weather on power grids. These include a power blackout

in Toronto in 1958 (Lanzerotti & Gregori 1986), outage of a communication cable system in the Midwest USA in 1972 (Anderson et al. 1974), a 9-hr blackout in Quebec in 1989 (i.e., the Quebec blackout storm), and a blackout in Sweden in 2003 (i.e., the Halloween storm). Oughton et al. (2017) argued that extreme space weather-induced blackouts can cost the US economy alone \$41.5 billion per day. Thus, in situ monitoring of space weather for accurate nowcasting and forecasting is essential to protect social properties and prevent unexpected costs.

Satellite-based in situ observations of the near-Earth space environment have made significant contributions toward a better understanding of space weather mechanisms. Since the launch of the Explorer 1 satellite, which discovered the Van Allen radiation belts (van Allen et al. 1959), many satellite-based space weather missions have been implemented (e.g., MAGSAT, CHAMP, POLAR). Recently, numerous satellites have been placed in geostationary orbit to provide continuous

© This is an Open Access article distributed under the terms of the Creative Commons Attribution Non-Commercial License (<https://creativecommons.org/licenses/by-nc/3.0/>) which permits unrestricted non-commercial use, distribution, and reproduction in any medium, provided the original work is properly cited.

Received 9 JULY 2018 Revised 30 AUG 2018 Accepted 31 AUG 2018**[†]Corresponding Author**Tel: +82-43-717-0235, E-mail: aceasia@korea.krORCID: <https://orcid.org/0000-0003-2691-804X>

weather monitoring, uninterrupted communication services, and many other social infrastructures for concentrated regions. The space weather environment at geostationary orbit is highly dynamic and easily affected by extreme phenomena such as energetic particle exposure or geomagnetic storms. Thus, the geostationary orbit should be monitored to prevent damage from space weather events.

Los Alamos National Laboratory (LANL) satellites measured energetic particle distributions at geostationary orbit from 1989 to 2016. The National Oceanic and Atmospheric Administration (NOAA)'s Geostationary Operational Environmental Satellite (GOES) series (Menzel & Purdom 1994) has operated the Space Environment Monitor (SEM) since GOES-12 (GSFC 1996). Himawari-8 and -9, which are part of Japan's geostationary meteorological satellite series (Bessho et al. 2016), has installed a space environment data acquisition (SEDA) monitor. China first launched the geostationary satellite Fengyun (FY)-2 series, which includes an SEM, in 1997. On December 11, 2016, they launched the FY-4A satellite that included a space environment package (SEP) as a payload (Yang et al. 2017). Upcoming launches in the FY-4 satellite series will send additional SEPs into geostationary orbit. While the energetic particle detector and magnetometer are the most essential components for monitoring space weather, satellite-based magnetometers must address magnetic noise from the spacecraft body, which is a costly and complicated task (Acuña 2002). This is one reason why the Himawari-8/9 and FY-2 series do not include a magnetometer. Table 1 briefly summarizes current geostationary satellites and their space weather instruments.

The GeoKompsat-2A (GK-2A) is a new generation of Korean geostationary meteorological satellite that will be launched at the end of 2018. The GK-2A involves a Korea Space wEather Monitor (KSEM), which is a suite of space weather monitoring instruments. The purpose of the KSEM mission is to provide real-time monitoring of space from the eastern hemisphere. KSEM consists of a particle detector (PD), magnetometer (MG), and charging monitor (CM) (Fig. 1). The PD has 128 energy channels for electrons and protons; it measures their fluxes in an energy range of 100 keV-2 MeV. The MG measures a magnetic field of $\pm 64,000$ nT along three axes. The KSEM MG uses a service-oriented spacecraft magnetometer (SOSMAG) system with a 1-m-long deployable boom to reduce disturbance from the satellite body. This is a remarkably short length compared to other satellite-based MG booms. The CM is for direct monitoring of the satellite's internal charging, and its products will be used for cross-verification with PD data. Table 2 lists the specifications of the sensors. The data from those sensors will be used to produce more advanced and

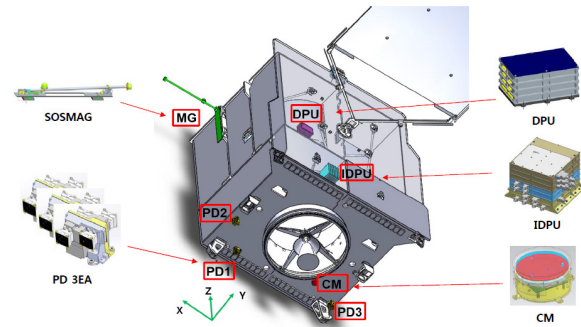


Fig. 1. GK-2A and KSEM instruments. The IDPU for all KSEM instruments and DPU for SOSMAG are located in the satellite body. The Z-axis is towards Earth. Each PD has a different position and angle of view. The DPU, IDPU, and two AMR magnetometers are located inside the satellite body. The SOSMAG uses a deployable boom.

Table 1. Space weather instruments of recent geostationary satellite

Satellites	Instruments and products	Launch
GOES 13/14/15 (USA)	XRS Solar X-ray flux EPS Energetic particle flux EUVS Extreme ultraviolet flux MAG Magnetic field	2006 (GOES 13) 2009 (GOES 14) 2010 (GOES 15)
GOES 16/17 (USA)	EXIS Extreme ultraviolet and X-ray flux SUVI Solar ultraviolet images SEISS Energetic particle flux MAG Magnetic field	2016 (GOES 16) 2018 (GOES 17, latest)
FY-2 series (China)	SEM Energetic particle flux Solar X-ray fluxes	2004 (FY-2C) 2018 (FY-2H, latest)
FY-4A (China)	SEP Energetic particle flux Magnetic field Solar images	2016
Himawari-8/9 (Japan)	SEDA Energetic particles	2014 (Himawari-8) 2016 (Himawari-9)
LANL series (USA)	MPA Magnetospheric plasma SOPA, ESP Energetic particle flux	1989 (LANL-89) 2002 (LANL-02A, latest)
GK-2A (Korea)	KSEM Energetic particle flux Magnetic field Satellite internal charging	2018

Table 2. Summary of sensors equipped on the KSEM

Satellites	Parameter	Specification
PD	Energy range	100 keV \leq E \leq 2 MeV
	Energy resolution	$\Delta E/E \leq 0.2\%$
	Time resolution	≤ 0.33 sec
	View direction	six directions
	Count resolution	8 bit
MG	Range	± 350 nT
	Accuracy	≤ 1 nT
	Time resolution	0.1 sec
	Boom length	1 m
CM	Range	-3 pA/cm ² to + 3pA/cm ²
	Accuracy	≤ 0.01 pa/cm ²
	Time resolution	≤ 0.1 sec

various level 2 data (see Section 3). This article describes the instruments and data applications of KSEM.

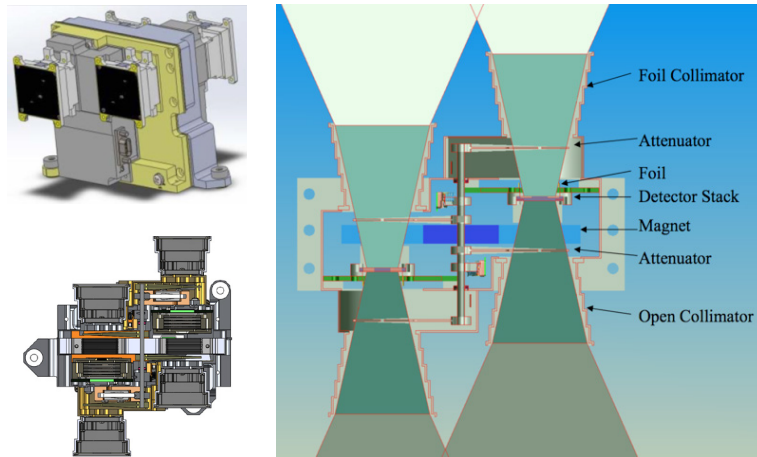


Fig. 2. Particle detector unit architecture. The PD design is based on the THEMIS SST, which has been proven to perform well in many space missions.

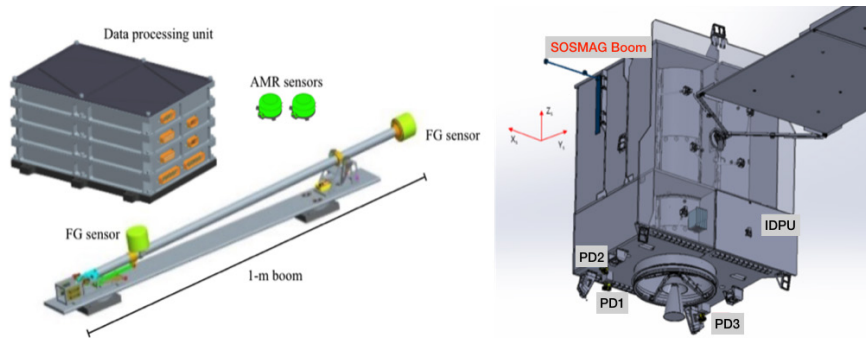


Fig. 3. SOSMAG magnetometer architecture. The SOSMAG consists of two fluxgate magnetometers on a 1-m-long boom, two AMR sensors inside the satellite body, and a data processing unit. The boom is deployed at the beginning of the commissioning phase.

2. KSEM OVERVIEW

2.1 Particle Detector

The KSEM PD uses a solid-state detector (SSD), which follows the instrument heritage from satellite-based PDs on WIND, STEREO, THEMIS, and MAVEN. The KSEM PD consists of three independent solid-state telescope (SST) units (Fig. 2). Each unit has two double-sided heads to measure both electrons and protons in opposite directions. While the THEMIS SST, which flies nearby in geostationary orbit, measures the energetic particle flux from 20 keV to 1 MeV every 3 sec (Angelopoulos 2008), the KSEM PD can measure energetic electron or proton fluxes from 100 keV to 2 MeV at a higher temporal resolution (≤ 0.33 sec).

In the electron detecting head (F side), protons at <300 keV are filtered out by a thin Al-polyamide-Al foil ahead of the foil (F) detector. In the proton detecting head (O side), electrons at <300 keV are swept away by the Sm-Co magnet ahead of the open (O) detector. Between the F and

O detectors, there are two additional thick (T) detectors to resolve particles at >300 keV; each consists of three detectors wired in parallel. Cross-contamination by >300 keV protons on the F side and by >300 keV electrons on the O side is corrected using a decontamination matrix obtained from Geant 4 simulation results (Agostinelli et al. 2003).

While protons require high energy above 5 MeV to penetrate through 0.1-mm-thick aluminum shielding or 0.3-mm-thick Kapton material, low- to medium-energy electrons (100 keV–2 MeV) can infiltrate the satellite and increase the potential for electrostatic discharge (ESD) (Ferguson et al. 2011). One of the most recent critical satellite anomalies, reported by Loto'aniu et al. (2015), occurred when the Galaxy 15 geostationary satellite experienced a loss of control and stopped responding to the ground on April 5, 2010, resulting in the highest flux of 75–475 keV electrons to date since 2009. In contrast, the fluxes of higher-energy electrons (>0.8 MeV) and protons (>6.5 MeV) did not show any significant increase (Loto'aniu et al. 2015). Hence, the energy range of 100 keV–2 MeV should be prioritized for monitoring.

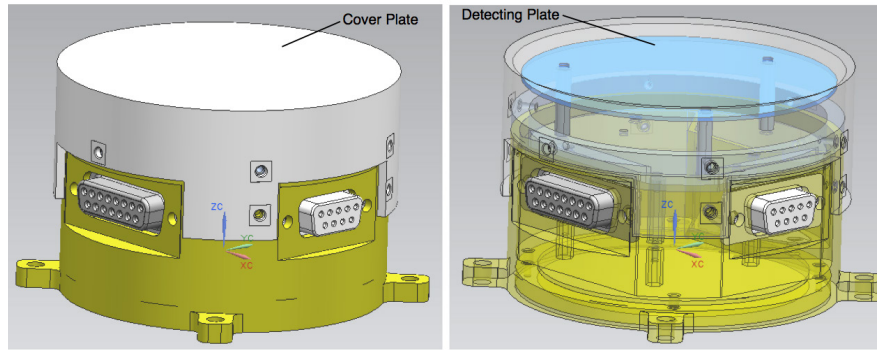


Fig. 4. Charging monitor architecture. CM has aluminum housing to prevent proton contamination and a charge collecting Al-plate inside (detecting plate). The CM concept is based on the engineering radiation monitor in the Van Allen probes (Goldsten 2013) and SURF in the Merlin Giove-A satellite (Taylor et al., 2007)

2.2 Magnetometer

The magnetic cleanliness of the satellite body is one of the key parameters for in situ magnetic field measurements. In practice, it is not possible to make a perfectly magnetically clean satellite body; most satellite-based magnetometers use booms several meters long, which can affect the overall satellite design and flight operation. SOSMAG enables detection and elimination of intrinsic electromagnetic noise caused by the alternating current (AC) from the satellite body. It contains dual fluxgate magnetometers on a 1-m-long boom and two AMR sensors inside the satellite body, which monitor internal AC disturbers. The SOSMAG onboard system estimates the total effect of noise from the satellite body while continuously and simultaneously providing AC-cleaned magnetic field data. This makes it possible to simplify the magnetic cleanliness requirement and reduce the boom length. The achieved AC noise correction accuracy is ± 0.1 nT, which is high enough for in situ monitoring and analysis of space weather. See Auster et al. (2016) for more details on the SOSMAG algorithm.

While every MG has its own sensor offset that can be measured during the ground test, the offsets in orbit should also be continuously re-measured and optimized because the extreme environment of space can alter the sensor offsets (Balogh et al. 2001). The most typical method for measuring sensor offsets is to spin the satellite along two axes under the assumption that the magnitude and direction of the background magnetic field are constant during spinning (Acuña 2002; Acuña et al. 2008). To provide continuous real-time monitoring, GK-2A will be a three-axis stabilized satellite. Thus, alternative methods are required. GOES satellites share the same geostationary orbit as GK-2A and have been monitoring the magnetic field of this orbit for many years. The long-term averages of GOES MG data during non-storm periods and Tsyganenko geomagnetic

field models (Tsyganenko & Sitnov 2007) are used as reference data to estimate the magnetic background value and offset from the AC-cleaned MG data.

Experimental methods considered include using magnetic compressional fluctuations such as Alfvén waves (Alfvén 1942) and drift mirror-mode waves (Hasegawa 1969; Tsurutani et al. 1982). This method is based on the Davis-Smith method (Davis Jr. & Smith 1968), for which further improvements have been presented in many studies (e.g., Leinweber et al. 2008; Leinweber 2011; Pudney et al. 2012; Bentley et al. 2016).

2.3 Charging Monitor

The KSEM CM monitors the satellite internal charging as a satellite housekeeping element. It has aluminum housing to prevent proton contamination and a charge collecting plate inside (Fig. 4). To resolve a weak current with less noise, an onboard OP-amp converts and amplifies a weak current (on the order of a few picoamperes) to a noticeably high voltage (10s–100s mV). Because CM data are used to obtain the satellite charging index, which can also be obtained independently from PD data, they can verify each other.

3. APPLICATION OF KSEM DATA

3.1 Space Weather Products

KSEM level 1 data (i.e., high energy particle flux, magnetic field along three axes, and satellite internal charging) can be used to produce five types of level 2 data: the magnetospheric particle flux (MPF), geostationary electron flux (GEF) prediction, satellite charging (SC) index, Kp index prediction (KIP), and Dst index prediction (DIP) (Table

Table 3. KSEM Level 2 product summary. a: Magnetospheric Particle Flux, b: GEO Electron Flux Prediction, c: Satellite Charging, d: Kp Index Prediction, e: Dst Index Prediction

Product	Period	Resolution	Products
MPFa	1 hr	0.2 Re	Particle flux in magnetosphere
GEFb	1 hr	1 hr	Particle flux prediction at geostationary orbit
SCc	1 hr	1 hr	Internal charging index of the satellite
KIPd	1 hr	3 hr	Kp index prediction
DIPe	1 hr	1 hr	Dst index prediction

Table 4. Energy channels of the MPF

Channel	Energy band
E1	>100 keV
E2	>494 keV
E3	>1098 keV
E4	>1637 keV
E5	>2000 keV

Table 5. Energy channels of the GEF

Channel	Energy band
E1	>100 keV
E2	>122 keV
E3	>149 keV
E4	>182 keV
E5	>222 keV
E6	>271 keV
E7	>331 keV
E8	>404 keV
E9	>494 keV
E10	>603 keV
E11	>736 keV
E12	>899 keV
E13	>1098 keV
E14	>1341 keV
E15	>1637 keV
E16	>2000 keV

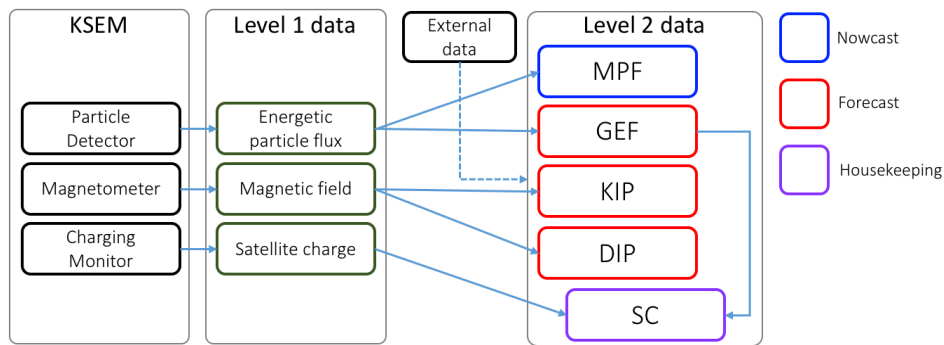


Fig. 5. Schematic of KSEM data process. MPF: magnetospheric particle flux, GEF: GEO electron flux prediction, SC: satellite charging, KIP: Kp index prediction, DIP: Dst index prediction.

3 and Fig. 5). The algorithms for the GEF and DIP utilize additional data from the GOES series to improve prediction performance. Details of the algorithms are described in additional papers currently being prepared and soon to be submitted. We describe these algorithms briefly here.

Magnetospheric Particle Flux. MPF is the estimated electron flux for the entire magnetosphere in five energy channels (Table 4; KASI & ETRI 2016d). It provides electron fluxes at $L=2-7$ in intervals of 0.2. The MPF algorithm also uses solar wind data, the Kp index, and the Dst index as external inputs for the Tsyanenko model (Tsyanenko & Sitnov 2007). The algorithm combines the external data and KSEM PD data, then estimate real-time particle distribution in the earth’s magnetosphere by solving the on-dimensional Fokker-Plank diffusion equation that is typically used for the earth’s radiation belt models (e.g., Shin et al. 2014). The algorithm is based on the versatile electron radiation belt (VERB) code developed by the Radiation Belt Modeling Group of The University of California (Subbotin & Shprits 2009, Shprits et al. 2009), but is simplified and has faster run

time than the original code. A three-dimensional particle distribution is drawn from MPF data.

Geostationary Electron Flux Prediction. GEF is the estimated electron flux at geostationary orbit in 16 energy channels (Table 5; KASI & ETRI 2016b). The GEF neural network algorithm predicts the electron flux over a geostationary equatorial orbit (GEO) up to 12 hr in advance in 1-hr intervals while maintaining sufficient accuracy. Using external data from a GOES-East satellite on the opposite side of GK-2A allows GEF to produce a 24-hr prediction with better reliability than using a single spot measurement. GEF data can be used to obtain real-time particle environments around individual geostationary satellites such as the FY series, Himawari-8/9, and GOES-West.

Satellite Charging. SC is the estimated internal current caused by high-energy plasma near a geostationary satellite (KASI & ETRI 2016e). It provides the charging index of a 0.2–2.0 mm thick aluminum shield at 0.2-mm increments and predicts the SC 1–24 hr in advance at 1-hr intervals. The SC algorithm uses GEF prediction values as input data.

Kp Index Prediction. KIP predicts the Kp index 1–24 hr in advance in 3-hr intervals (KASI & ETRI 2016c). The KIP algorithm consists of empirical formulas and neural networks and uses magnetic field data at geostationary orbit.

Dst Index Prediction. DIP is the estimated Dst index, and the algorithm consists of empirical formulas and neural networks that use magnetic field data at geostationary orbit (KASI & ETRI 2016a). The algorithm uses magnetic field data over an entire GEO orbit. With a single spot measurement, it must use 24-hr-old data that could have different values in the present. To address this, the algorithm also uses data from two GOES satellites. By combining data from three satellites in the same orbit, past data are a maximum of 14 hr old. The DIP algorithm predicts the Dst index 1–14 hr in advance in 1-hr intervals.

3.2 KSEM Contribution to Improving Science and Space Weather Services

KSEM level 2 products are designed for space weather monitoring and forecasting. However, simultaneous multipoint observations conducted in a geostationary orbit have value beyond the field of forecasting.

A number of studies have indicated that the space weather environment at geostationary orbit has an asymmetric and responsive configuration. Borodkova et al. (2008) showed that the amplitude of the geostationary response is dependent on the observer’s location relative to the noon meridian. Lee & Lyons (2004) found that the geostationary response of the magnetosphere to the solar wind dynamic pressure (P_d) depends on the orientation of the interplanetary magnetic field (IMF). Sanny et al. (2002) suggested that the variability of the magnetic field strength around local noon at a geostationary orbit has a stronger correlation with P_d than the direction of IMF Bz. Wing & Sibeck (1997) demonstrated that the geostationary magnetic Bz has different dayside and nightside responses to increasing P_d . Dong et al. (2014) found that the southward turning of the IMF Bz may increase the geostationary magnetic field in the dawn sector. These results indicate that the dynamics of the geomagnetic field and interplanetary magnetic field are strongly coupled and that a geostationary orbit is a suitable location for observing and studying planetary physics around the Earth. Two GOES satellites separated by approximately 4 hr local time can provide parameters of solar wind P_d for approximately 10 hr each day (Singer et al. 1996). The longitude of GK-2A is 128.2°E, while those of the GOES satellites are 75°W and 135°W. A combination of these three GEO satellites could allow P_d

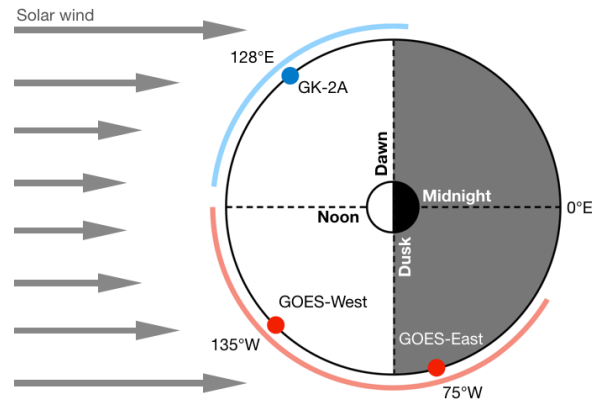


Fig. 6. Schematic of GK-2A and GOES satellites orbital positions. Two GOES satellites separated by approximately 4 hr local time provide an indicator of solar wind P_d during ~10 hr each day (red circles and line, Sing et al., 1996). With GK-2A, under the same conditions (blue circle and line), the total monitoring duration of P_d could be expanded by more than half a day.

monitoring for almost 13 hr each day (Fig. 6).

The geostationary orbit is near the plasmapause, where the density of cold plasma has a very sharp gradient (Kwon et al. 2015). The size and shape of the plasmasphere have a complex relationship with the solar wind and near-Earth magnetic activity. Thus, a geostationary orbit is one of the best locations to observe plasmasphere dynamics.

While the above studies reveal the need for systematic monitoring in a geostationary orbit, most geomagnetic studies use GOES satellites, which only cover part of the orbit. Previous studies essentially depended on comparing several similar events that occurred when the satellite was in a different position. LANL satellites provided more observation points, but their data update stopped in 2016. GK-2A is located on almost the opposite side of GOES-East in a geostationary orbit. KSEM on GK-2A can simultaneously observe and provide real-time information on the configuration and temporal variation of the other half of the geomagnetic environment. This can facilitate further quantitative studies and provide a better understanding of the interaction and dynamics of the geomagnetic field and IMF.

Empirical magnetosphere modeling is key for studying the magnetic field response to solar wind and tracing plasma waves and energetic particles around the Earth. The reliability of empirical magnetosphere models is intrinsically dependent on obtaining as much in situ data on conditions and fluctuations as possible. Tsyganenko & Sitnov (2005) introduced one of the most refined empirical models (TS05). The addition of 37 magnetic storm events to the dataset used to fit the model coefficients allowed TS05 to successfully and efficiently reproduce storm-time field magnitudes and configurations, even during strong storm

activity (Huang et al. 2008). Andreeva & Tsyganenko (2018) developed a model to describe the magnetic field around a geostationary orbit. To validate the model with actual in situ data, they used GOES-15 data, which originate from a single spot during each event. More data spots will obviously result in more accurate validation. Thus, GK-2A's KSEM should effectively contribute towards building and validating a better empirical magnetosphere model by providing more event data measured simultaneously with the GOES series.

4. CONCLUSION

KSEM/GK-2A represents new capabilities for in situ space weather monitoring systems in a geostationary orbit. More accurate real-time nowcasting and more reliable forecasting will be available with KSEM's high-precision measurement of energetic particle fluxes and the magnetic field. The geostationary orbit is the most dynamic region of the magnetosphere, exhibiting unique properties. Thus, systematic monitoring of this orbit is critical from both practical and scientific aspects. At present, space weather monitoring at geostationary orbit, especially of the magnetic field, mostly depends on data from the GOES satellite series, whose coverage is limited to the western hemisphere. KSEM/GK-2A data will cover the eastern hemisphere, which has so far been an observational blind spot. This represents a valuable expansion in observations, enabling simultaneous multi-point monitoring from both sides of the Earth. A continuous, global, and simultaneous observation system consisting of KSEM/GK-2A, GOES, and other planned GEO satellites, such as the Fengyun-4 series of China (Yang et al. 2017), presents outstanding advantages for revealing space weather mechanisms and improving space weather prediction.

ACKNOWLEDGMENTS

This study was funded by the KMA/NMSC (Korea Meteorological Administration/National Meteorological Satellite Center) R&D Project (NMSC-2016-3137). The authors thank Dr. Nikolai Tsyganenko, who provided valuable opinions on the KSEM/GK-2A project.

REFERENCES

Acuña MH, Space-based magnetometers, *Rev. Sci. Instrum.* 73, 3717 (2002). <https://doi.org/10.1063/1.1510570>

- Acuña MH, Curtis D, Scheifele JL, Russell CT, Schroeder P, et al., The STEREO/IMPACT magnetic field experiment, *Space Sci. Rev.* 136, 203-226 (2008). <https://doi.org/10.1007/s11214-007-9259-2>
- Agostinelli S, Allison J, Amako K, Apostolakis J, Araujo H, et al., GEANT4—a simulation toolkit, *Nucl. Instrum. Methods Phys. Res. A* 506, 250-303 (2003). [https://doi.org/10.1016/S0168-9002\(03\)01368-8](https://doi.org/10.1016/S0168-9002(03)01368-8)
- Alfvén H, Existence of electromagnetic-hydrodynamic waves, *Nature* 150, 405-406 (1942). <https://doi.org/10.1038/150405d0>
- Anderson CW, Lanzerotti LJ & MacLennan CG, Outage of the L-4 system and the geomagnetic disturbance of August 4, 1972, *Bell Syst. Tech. J.* 53, 1817-1837 (1974). <https://doi.org/10.1002/j.1538-7305.1974.tb02817.x>
- Andreeva VA, Tsyganenko NA, Empirical modeling of the quiet and storm time geosynchronous magnetic field, *Space Weather* 16, 16-36 (2018). <https://doi.org/10.1002/2017SW001684>
- Angelopoulos, The THEMIS mission, *Space Sci. Rev.* 141, 5-34 (2008). <https://doi.org/10.1007/s11214-008-9336-1>
- Auster U, Magnes W, Delva M, Valavanoglou A, Leitner S, et al., Space weather magnetometer set with automated AC spacecraft field correction for Geo-Kompsat-2A, in 2016 ESA Workshop on Aerospace EMC, Valencia, Spain, 23-25 May 2016.
- Balogh A, Planetary magnetic field measurements: missions and instrumentation, *Space Sci. Rev.* 152, 23-97 (2010). <https://doi.org/10.1007/s11214-010-9643-1>
- Bentley J, Sheppard D, Rich F, Redmon R, Loto'aniu P, et al., Exploring the use of Alfvén waves in magnetometer at geosynchronous orbit, in 2016 AGU Fall Meeting; 12-16 Dec 2016.
- Borodkova NL, Liu JB, Huang ZH, Zastenker GN, Geosynchronous magnetic field response to the large and fast solar wind dynamic pressure change, *Adv. Space Res.* 41, 1220-1225 (2008). <https://doi.org/10.1016/j.asr.2007.05.075>
- Choi HS, Lee J, Cho KS, Kwak YS, Cho IH, et al., Analysis of GEO spacecraft anomalies: space weather relationships, *Space Weather* 9, S06001 (2011). <https://doi.org/10.1029/2010SW000597>
- Davidson WF, The magnetic storm of March 24, 1940 - Effect in the power system, *Edison Elect. Inst. Bull.* 365-366 & 374 (1940).
- Davis Jr. L, Smith EJ, The in-flight determination of spacecraft magnetic field zeros, *EOS Trans. AGU.* 49, 257 (1968).
- Dong YX, Cao JB, Liu WL, Zhang L, Li LY, Response of magnetic fields at geosynchronous orbit and on the ground to the sudden changes of IMF B_z , *Sci. China Tech Sci.* 57, 360-367 (2014). <https://doi.org/10.1007/s11431-013-5428-6>

- Ferguson DC, Denig WF, Rodriguez JV, plasma conditions during the Galaxy 15 anomaly and the possibility of ESD from subsurface charging, Proceedings of the 49th AIAA Aerospace Science Meeting including the New Horizons Forum & Aerospace Exposition, Orlando, FL, 4-7 January 2011.
- GSFC, GOES I-M DataBook: 1996 (NASA GSFC, Greenbelt, 1996).
- Goldsten JO, Maurer RH, Peplowski PN, Holmes-Siedle AG, Herrmann CC, et al., The engineering radiation monitor for the radiation belt storm probes mission, Space Sci. Rev. 179, 485-502 (2013). <https://doi.org/10.1007/s11214-012-9917-x>
- Hasegawa A, Drift mirror instability of the magnetosphere, Phys. Fluids 12, 2642 (1969). <https://doi.org/10.1063/1.1692407>
- Huang CL, Spence HE, Howard JS, Tsyganenko NA, A quantitative assessment of empirical magnetic field models at geosynchronous orbit during magnetic storms, J. Geophys. Res. 113, A04208 (2008). <https://doi.org/10.1029/2007JA012623>
- KASI, ETRI, GEO-KOMPSAT-2A Dst Index Prediction Algorithm Theoretical Basis Document, KASI & ETRI, Version 1.0 (2016a).
- KASI, ETRI, GEO-KOMPSAT-2A Electron Flux Prediction Algorithm Theoretical Basis Document, KASI & ETRI, Version 1.1 (2016b)
- KASI, ETRI, GEO-KOMPSAT-2A Kp Index Prediction Algorithm Theoretical Basis Document, KASI & ETRI, Version 1.0 (2016c)
- KASI, ETRI, GEO-KOMPSAT-2A Magnetospheric Particle Environment Algorithm Theoretical Basis Document, KASI & ETRI, Version 0.1 (2016d)
- KASI, ETRI, GEO-KOMPSAT-2A Spacecraft Charging Monitor Algorithm Theoretical Basis Document, KASI & ETRI, Version 0.1 (2016e)
- Kwon HJ, Kim KH, Jee G, Park JS, Nishiyama Y, Plasmopause location under quiet geomagnetic conditions ($Kp \leq 1$): THEMIS observations, Geophys. Res. Lett. 42, 7303-7310 (2015). <https://doi.org/10.1002/2015GL066090>
- Lanzerotti LJ, Gregori GP, Telluric currents: the natural environment and interactions with man-made systems, The Earth's Electrical Environment, eds. Roble RG, Krider EP (National Academy Press, Washington D.C., 1986), 232-257.
- Lee DY, Lyons LR, Geosynchronous magnetic field response to solar wind dynamic pressure pulse, J. Geophys. Res. 109, A04201 (2004). <https://doi.org/10.1029/2003JA010076>
- Leinweber HK, Russell CT, Torkar K, Zhang TL, Angelopoulos V, An advanced approach to finding magnetometer zero levels in the interplanetary magnetic field, Meas. Sci. Technol. 19, 055104 (2008). <https://doi.org/10.1088/0957-0233/19/5/055104>
- Leinweber HK, In-flight Calibration of Space-borne Magnetometers, PhD dissertation, Graz University of Technology, (2011).
- Lohmeyer WQ, Cahoy K, Space weather radiation effects on geostationary satellite solid-state power amplifiers, Space Weather 11, 476-488 (2013). <https://doi.org/10.1002/swe.20071>
- Loto'aniu TM, Singer HJ, Rodriguez JV, Green J, Denig W, et al., Space weather conditions during the Galaxy 15 spacecraft anomaly, Space Weather 13, 484-502 (2015). <https://doi.org/10.1002/2015SW001239>
- Menzel WP, Purdom JFW, Introducing GOES-I: the first of a new generation of geostationary operational environmental satellites, Bull. Am. Meteorol. Soc. 75, 757-782 (1994). [https://doi.org/10.1175/1520-0477\(1994\)075<0757:IGITFO>2.0.CO;2](https://doi.org/10.1175/1520-0477(1994)075<0757:IGITFO>2.0.CO;2)
- Nicholson SB, The great magnetic storm of march 24, Publ. Astron. Soc. Pac. 52, 169-171 (1940).
- Oughton EJ, Skelton A, Horne RB, Thomson AWP, Gaunt CT, Quantifying the daily economic impact of extreme space weather due to failure in electricity transmission infrastructure, Space Weather 15, 65-83 (2017). <https://doi.org/10.1002/2016SW001491>
- Pudney MA, Carr CM, Schwartz SJ, Howarth SI, Automatic parameterization for magnetometer zero offset determination, Geosci. Instrum. Method. Data Syst. 1, 103-109 (2012). <https://doi.org/10.5194/gi-1-103-2012>
- Sanny J, Tapia JA, Sibeck DG, Moldwin MB, Quiet time variability of the geosynchronous magnetic field and its response to the solar wind, J. Geophys. Res. 107, 443 (2002). <https://doi.org/10.1029/2002JA009448>
- Shin DK, Lee DY, Kim JH, Cho JH, Prediction model of the outer radiation belt developed by Chungbuk National University, J. Astron. Space Sci. 31, 303 (2014). <https://doi.org/10.5140/JASS.2014.31.4.303>
- Shprits YY, Subbotin D, Ni B, Evolution of electron fluxes in the outer radiation belt computed with the VERB code, J. Geophys. Res., 114, A11209 (2009). <https://doi.org/10.1029/2008JA013784>
- Singer H, Matheson L, Grubb R, Newman A, Bouwer D, Monitoring space weather with the GOES magnetometers, Proceeding of the SPIE's 1996 International Symposium on Optical Science, Engineering, and Instrumentation, Denver, CO, 4-9 August 1996.
- Subbotin DA, Shprits YY, Three-dimensional modeling of the radiation belts using the Versatile Electron Radiation Belt (VERB) code, Space Weather 7, S100001 (2009). <https://doi.org/10.1029/2008SW000452>

- Taylor B, Underwood CI, Evans HDR, Ryden K, Rodgers D, et al., Results from the Galileo Giove—a radiation monitors and comparison with existing radiation belt models, *IEEE Trans. Nucl. Sci.* 54, 1076-1081 (2007). <https://doi.org/10.1109/TNS.2007.892115>
- Tsurutani BT, Smith EJ, Anderson RR, Ogilvie KW, Scudder JD, et al., Lion roars and nonoscillatory drift mirror waves in the magnetosheath, *J. Geophys. Res.* 87, 6060-6072 (1982). <https://doi.org/10.1029/JA087iA08p06060>
- Tsyganenko NA, Sitnov MI, Magnetospheric configurations from a high-resolution data-based magnetic field model, *J. Geophys. Res.* 112, A06225 (2007). <https://doi.org/10.1029/2007JA012260>
- van Allen JA, McIlwain CE, Ludwig GH, Radiation observations with satellite 1958 ϵ , *J. Geophys. Res.* 64, 271-286 (1959). <https://doi.org/10.1029/JZ064i003p00271>
- Wing S, Sibeck DG, Effects of interplanetary magnetic field z component and the solar wind dynamic pressure on the geosynchronous magnetic field, *J. Geophys. Res.* 102, 7207-7216 (1997). <https://doi.org/10.1029/97JA00150>
- Yang J, Zhang Z, Wei C, Lu F, Guo Q, Introducing the new generation of chinese geostationary weather satellites, Fengyun-4, *Bull. Amer. Meteorol. Soc.* 98, 1637-1768 (2017). <https://doi.org/10.1175/BAMS-D-16-0065.1>

